Talanta 310 (2026) 130063

Contents lists available at ScienceDirect

Talanta

journal homepage: www.elsevier.com/locate/talanta

# Fluoro4Graphene: A fluorogenic high-throughput screening platform for property engineering of graphene binding peptides

Ines Vogt [a], Florian Bourdeaux [a], Tetiana Kurkina [a], Aidin Nikookhesal [b], Sven Ingebrandt [b], Vivek Pachauri [b], Ulrich Schwaneberg [a,*]

[a] RWTH Aachen University, Institute of Biotechnology, Worringerweg 3, Aachen, 52074, Germany
[b] RWTH Aachen University, Institute of Materials in Electrical Engineering 1, Sommerfeldstraße 24, Aachen, 52074, Germany

ARTICLE INFO

*Keywords:*
Graphene
Material binding peptides
Biofunctionalization
High-throughput screening
Directed evolution
Non-covalent functionalization

ABSTRACT

Experimental and quantitative methods for studying protein-graphene interactions remain limited, despite their importance for biosensing and biointerface engineering. Here, we report *Fluoro4Graphene*, a three-step high-throughput fluorescence-based screening assay for the identification of graphene-binding peptides. In this platform, candidate peptides are genetically fused to the phytase of *Yersinia mollaretti*, which serves as a reporter enzyme by converting 4-methylumbelliferyl phosphate into the fluorescent 4-methylumbelliferone. Robust signal quantification is achieved by transferring the soluble fluorophore to a secondary microtiter plate prior to detection, thereby avoiding graphene-induced fluorescence. The assay is performed directly from crude *Escherichia coli* lysates in microtiter plates coated with electrochemically exfoliated graphene flakes, eliminating protein purification steps and enabling high sample throughput. The platform exhibits good reproducibility, with a coefficient of variation of approximately 17%, allowing reliable discrimination of small differences in binding. Analytical performance was validated in a directed evolution campaign targeting the material binding peptide Macaque histatin-1, yielding variants with improved graphene surface coverage. The best variant showed a 1.44-fold improvement in the Fluoro4Graphene screening assay. Independent validation using surface plasmon resonance on high-purity graphene confirmed an increase in surface coverage from 106.19 ng/cm$^2$ to 154.10 ng/cm$^2$. Overall, Fluoro4Graphene provides a robust, reproducible, and scalable analytical tool for the quantitative assessment of protein–graphene interactions.

## 1. Introduction

Graphene is widely used in biotechnology and biomedicine due to its large surface-to-volume ratio and ability to interact with biomolecules [1]. For many applications, including biointerfaces and functional coatings, a quantitative understanding of protein-graphene binding is essential [2]. However, experimental methods to quantitatively and reproducibly determine protein binding to graphene in a high-throughput-compatible manner remain limited. Biophysical methods such as quartz crystal microbalance with dissipation monitoring (QCM-D), atomic force microscopy (AFM), and surface plasmon resonance (SPR) are unsuitable for screening hundreds of samples in typical directed evolution campaign timeframes [3–5].

Fluorescence-based screening methods are commonly used in high-throughput protein engineering. However, graphene is reported to quench fluorescence [6], which presents a significant limitation for fluorescence-based screening platforms using graphene surfaces. For instance, green fluorescent protein (GFP)-fusions [7,8] cannot be used for binding studies on graphene due to quenched GFP fluorescence [9]. Consequently, there is a strong need for alternative reporter systems that enable reliable signal generation independent of graphene-induced fluorescence quenching.

Graphene is a 2D nanomaterial with unique mechanical, electrical, and chemical properties due to its single-layer sp$^2$-hybridized carbon atoms, yielding π-π orbitals for delocalized electrons. The nanomaterial is optically transparent, whereas the C=C-network imparts extreme mechanical stiffness [10]. The extraordinarily high surface-to-volume ratio and chemical inertness make graphene-based materials (GBMs) ideal transducers, with exceptionally high sensitivity to thermal and electrochemical changes influencing their electrical conductivity [10,11]. Interestingly, some reports suggest that graphene displays biocompatible characteristics [12], leading to broad applications in

* Corresponding author.
*E-mail address:* u.schwaneberg@biotec.rwth-aachen.de (U. Schwaneberg).

https://doi.org/10.1016/j.talanta.2026.130063
Received 8 February 2026; Received in revised form 17 May 2026; Accepted 28 May 2026
Available online 9 June 2026

engineering, electrochemistry [13], biotechnology, and biomedicine; examples comprise tissue engineering [14], bioimaging [15], drug delivery [16], photothermal therapy [17], as well as highly sensitive biosensors [18]. For the above-mentioned applications, GBMs are required to undergo surface functionalization to employ desired functionalities, such as biomolecular receptors for analyte detection or enhanced cell adhesion [19–21]. Conventional functionalization strategies of GBMs can be divided into covalent and non-covalent bonding methodologies [22,23]. Covalent modification strategies for GBMs with a high C/O ratio, such as graphene, are often achieved through the reaction of radicals [24] or dienophiles [25]. However, using covalent functionalization perturbs the π-conjugated system, often resulting in unfavorable material characteristics such as low charge-carrier mobility and disparate optical properties [22,23]. The non-covalent methods for graphene functionalization are mainly based on adsorption through interactions with the extensive π-electron network, minimally impacting the characteristics of graphene [18,22,23,26]. Non-covalent immobilization methods typically use small aromatic molecules such as pyrene or its derivatives [22,26,27]. As an alternative to synthetic molecules, biological molecules, such as single-stranded nucleic acids (ssDNA) or peptides, can be used [22,26,27]. Aromatic bases within ssDNA bind via π-π stacking and hydrophobic interactions, while peptides can additionally bind via charged interactions [28–31]. Reports on biobased graphene coatings show possible improvement of biocompatibility and environmental performance of graphene and enable applications, such as drug delivery, tissue engineering, or biomarkers [32–35]. A challenge of non-covalent functionalization of graphene is the desorption of bound moieties [22].

Graphene-binding peptides have previously been identified by phage display methodologies or were synthesized de novo based on educated guesses or computational design [31,36–45]. As a general trend, the repetition of positively charged (predominantly arginine; histidine below pH 5 or lysine) or aromatic amino acids (e.g., tryptophan, tyrosine, histidine > pH 7) seems beneficial for graphene binding [28,31]. So far, the longest graphene-binding peptides identified by phage display are dodecapeptides [46].

Material binding peptides (MBPs) are small peptides (20 to 100 amino acids) capable of binding material surfaces from aqueous solutions [47,48]. They are classified as natural or engineered MBPs [46,47,49]. Unlike phage-display-derived peptides, MBPs have a defined domain/3D-structure that enable spatial recognition [46]. Their binding potential depends on sequence, structure, and charge, and includes inorganic, organic, and natural materials [7,50,51]. MBPs are compatible with scalable coating methods, such as dip and spray coating [46,52,53]. They can reach maximal surface coverage within 20 s on carbon nanotubes at ambient temperature [54].

A prominent MBP that binds to several polymers, such as polyethylene terephthalate, polyamide 6, polyamide 6.6, polyethylene, polypropylene, and polyvinyl chloride, is Macaque histatin 1 (MacHis) [55]. MacHis is a 38-amino acid-long histidine-rich peptide found in *Macaca fascicularis*, which exhibits antimicrobial and antifungal properties [56]. No NMR or crystal structure is known. Simulations such as AlphaFold suggest that there is no defined secondary structure [57]. Whereas TopModel suggests a helical-loop structure [51].

Protein engineering, through directed evolution or rational design, enables the adjustment of MBP properties to meet application demands, such as enhancing binding strength or enabling material-specific binding [46,51,58]. A prerequisite for the directed evolution of MBPs is a robust and reliable high-throughput compatible screening system. Such systems are routinely employed in directed evolution campaigns, usually with a coefficient of variation (CV) below 20% [58,59]. The directed evolution of an MBP for graphene has not yet been reported, largely due to the lack of suitable high-throughput analytical screening methods. Enzyme-based colorimetric or fluorogenic reporter systems, such as the phytase of *Yersinia mollaretti* (YmPh), offer a promising alternative [7]. Phytases catalyze the release of inorganic phosphate by hydrolysis of phytate [60]. Several substitute substrates, such as 4-methylumbelliferyl phosphate (4-MUP), can be used in the reaction. During 4-MUP hydrolysis, the fluorescent product, 4-methylumbelliferone (4-MU), is released into solution [61]. The fluorescent solution, transferred to a fresh microtiter plate, overcomes the quenching effects of graphene.

In this study, we developed and validated a robust high-throughput screening platform, named Fluoro4Graphene, to quantitatively measure the binding by the relative surface retention of a MBP (MacHis) on the surface using an analytical readout. The Fluoro4Graphene screening system is employed in a microtiter plate format (96 wells) and is based on 4-MUP and the YmPh as a reporter enzyme. Fluoro4Graphene comprises three steps: I: Plate coating with few-layered graphene flakes, II: Sample binding including the protein binding, and III: Signal detection. The robustness of the system was validated with a variant library of MacHis fused to YmPh. After the screening of 840 MacHis variants, 11 improved MacHis variants for binding on the surface of graphene were identified. Surface coverage was finally determined by SPR on high-purity graphene, confirming that a single substitution in MacHis can be quantitatively resolved for the selected screening conditions using the developed platform.

## 2. Experimental section

### 2.1. Materials

All used chemicals were purchased from AppliChem GmbH (Darmstadt, Germany), Carl Roth GmbH (Karlsruhe, Germany), and Sigma-Aldrich Chemie GmbH (Steinheim, Germany) with a purity of analytical-reagent grade or higher. Oligonucleotides were obtained from Eurofins Scientific SE (Ebersberg, Germany) in salt-free form. The GFP polyclonal antibody conjugated with horse radish peroxidase (catalogue number: 600-103-215) was purchased from Thermo Fisher Scientific Inc. (Waltham, Massachusetts, USA), and enzymes and enzyme mixes were purchased from New England Biolabs GmbH (Frankfurt am Main, Germany) or PCR Biosystems (London, England). Polymerase chain reaction purification and plasmid extraction kits were purchased from Macherey-Nagel GmbH & Co. KG (Düren, Germany). PP/Polyolefin 0.45 μm pore-sized PTFE filter plates were purchased from Merck Millipore (Burlington, Massachusetts, USA), and PS 96-well microtiter plates from Greiner Bio-One GmbH (Frickenhausen, Germany). Gold SPR chips were purchased from BioNavis Ltd (Tampere, Finland) and coated with single layer graphene film with grain size of up to 20 μm synthesized via CVD method on Cu foil (Cu thickness of 18 μm) (Raman Spectroscopy on each batch: I(G)/I(2D) < 1.25; I(D)/I(G) < 0.1 on 90 nm SiO2/Si substrate, Sheet Resistance on SiO2/Si: 350 ± 40 Ohms/sq (1 cm × 1 cm)) from Graphenea, Inc. (San Sebastian, Spain). Graphene dispersion (1 mg/mL in DMF, Graphene preparation method: electrochemical exfoliation, sheet size by AFM: micrometer range as stated by supplier, oxygen content: 7.5% (by XPS) (C/O-ratio: 12.3), Raman I_D/I_G ratio: 0.4, sheet resistance 4.8 kΩ/sq, average number of layers, 1 3) was purchased from Merck KGaA (Darmstadt, Germany).

### 2.2. Strain construction

The plasmids pALXtreme:YmPh-17xHelix-TEV-LCI, pALXtreme:YmPh-17xHelix-TEV-Cecropin A, and pALXtreme:YmPh-17xHelix-TEV-Tachystatin A2 were available in the group and are described in Ref. [60]. The plasmid pALXtreme:YmPh-17x-Helix-TEV was generated from pALXtreme:YmPh-17x-Helix-TEV-LCI, and pALXtreme:YmPh-17x-Helix-TEV-CBP1 was generated from pALXtreme:YmPh-17x-Helix-TEV by site-directed mutagenesis using the KLD-enzyme Kit from New England Biolabs GmbH (Frankfurt am Main, Germany). The plasmid pALXtreme:YmPh-17x-Helix-TEV-MacHis was obtained by homologous recombination of pALXtreme:YmPh-17xHelix-TEV-LCI and pET28(+):StrepII-eGFP-17xHelix-TEV-MacHis in *E. coli* DH5α [62] from Invitrogen (Karlsruhe,

Germany). *E. coli* BL21-Gold (DE3) lacI$^{Q1}$ (in-house) cells were transformed with these plasmids by heat shock according to the protocol given by New England Biolabs GmbH (Frankfurt am Main, Germany). The primer and amino acid sequences of proteins can be found in Tables S1 and S2.

#### 2.2.1. MacHis-library construction

The YmPh-MacHis library was generated by epPCR using the primers as described in Table S1, Taq-Polymerase, and 0.3 mM $MnCl_2$ for diversity generation of the gene encoding MacHis in 30 rounds. PCR fragments were used as megaprimers to perform the MEGAWHOP method with pALXtreme:YmPh-17x-Helix-TEV-MacHis as the template [63].

### 2.3. Expression of the MacHis library

Freshly transformed single colonies were picked from agar plates and used to inoculate 96-F-bottom-well plates from Greiner Bio-One GmbH (Frickenhausen, Germany) with 150 µL of LB-medium (yeast extract 10 g/L, tryptone 5 g/L, NaCl 5 g/L) containing 50 µg/mL carbenicillin in each well. Each plate contained, in addition to the variants, four positive controls, YmPh-MacHis WT, four negative controls, YmPh (no MBP), and four sterility controls. Precultures were incubated in an Infors AG (Bottmingen, Switzerland) HT Multitron incubator (900 rpm, 8 h, 37 °C, 60% humidity). 5 µL of the preculture was transferred into 96-V-bottom well plates containing 145 µL of ZYM-medium [64] with 50 µg/mL carbenicillin, incubated in an Infors AG (Bottmingen, Switzerland) HT incubator (900 rpm, 16 h, 37 °C, 60% humidity), and harvested by centrifugation in the Eppendorf SE (Hamburg, Germany) centrifuge 5810R (3200 rcf, 10 min, 4 °C). The supernatant was discarded, and the pellets were stored at −20 °C for further use.

### 2.4. Expression and purification of YmPh-MacHis variants

5 mL of 50 µg/mL carbenicillin-containing medium was inoculated with the variant-expressing strain directly from a cryoculture. Cultures were incubated in an Infors AG (Bottmingen, Switzerland) HT incubator (200 rpm, 8 h, 37 °C). For expression, 2 mL of the preculture was transferred to a flask with 200 mL of 50 µg/mL carbenicillin containing ZYM-Medium [99] and incubated in an Infors AG (Bottmingen, Switzerland) HT incubator (200 rpm, 16 h, 37 °C). Cells were harvested by centrifugation in the Thermo Fisher Scientific Inc. Sorvall RC 6+ (4000 rcf, 10 min, 4 °C) (Waltham, Massachusetts, USA). The supernatant was discarded, and the pellets were stored at −20 °C until further use. For purification, pellets were resuspended in 10 mL of Tris-HCl buffer (pH 8, 50 mM) and sonicated (65% amplitude, 5 min on, 15 s/15 s on-off cycles) with the ultrasonic processor Vibra Cell VCX 130 from Sonics & Materials, Inc. (Newton, Connecticut, USA). Lysate was centrifuged in an Eppendorf SE (Hamburg, Germany) centrifuge 5810R (11,000 rcf, 30 min, 4 °C). The supernatant was filtered through a filter with a pore size of 0.2 µm and loaded onto a 1 mL Ni-IDA 1000-column from Macherey-Nagel GmbH & Co. KG (Düren, Germany). Flowthrough was discarded, and the column was washed with 5 mL 20 mM imidazole in Tris-HCl buffer (pH 8, 50 mM). Flowthrough was discarded, and protein was eluted with 3 mL 400 mM imidazole in Tris-HCl buffer (pH 8, 50 mM). The eluate was loaded onto an equilibrated PD-10 Sepharose column from Cytiva (Marlborough, Massachusetts, USA) and eluted with 3 mL Tris-HCl buffer (pH 8, 50 mM). The protein was stored at 4 °C until further usage.

### 2.5. Fluoro4Graphene system, including coating, binding, and detection

I Coating: 0.45 µm pore-sized PTFE filter plates from Merck Millipore (Billerica, Massachusetts, USA) were blocked with 5% BSA in TBST (50 mM Tris-HCl pH 8, 150 mM NaCl, 0.05% Tween), 16 h, 4 °C). The blocking agent was filtered using a vacuum pump (350 mbar for 15 s), followed by the addition of 100 µL of 20 µg/mL graphene in 5% BSA TBST, which was then filtered through the plate. The graphene surface was dried at 65 °C for 3 h. II Binding: Cell pellets were resuspended and lysed by adding 150 µL of Lysozyme (1.5 mg/mL) and DNase1 (25 µg/mL) in 5% BSA TBST and incubated (37 °C, 900 rpm, 1 h). The lysate was centrifuged in an Eppendorf SE (Hamburg, Germany) centrifuge 5810R (3200 rcf, 30 min, 4 °C). The cleared supernatant was diluted (175 µL 5% BSA TBST + 75 µL lysate) and added to the graphene-coated plate. For the binding reaction, the plate was incubated (15 min, 500 rpm, 25 °C). Excess protein was washed away by 500 µL Tris-HCl buffer (pH 8, 50 mM) each in three wash cycles (5 min, 500 rpm, 25 °C). III Detection: 150 µL of 1 mM 4-MUP in sodium acetate buffer (50 mM, pH 5) was added to the plate in 10 s steps between each row. The reaction was incubated (20 min, 500 rpm, 25 °C). 100 µL of the solution was transferred to a black PS 96-well plate. Fluorescence was measured in the CLARIOstar Plus from BMG LABTECH GmbH (Ortenberg, Germany) (Ex: 360-20/Em: 450-30, gain 500). To normalize the signal 5 µL of undiluted crude lysate was added into a fresh black 96-well plate and mixed with 145 µL of 1 mM 4-MUP in sodium acetate buffer (50 mM, pH 5). Reaction and measurement were performed as above. Values from the crude lysate were used to normalize the values from the plates after the Fluoro4Graphene system.

### 2.6. Surface plasmon resonance (SPR) measurements

SPR gold chips were bought from BioNavis Ltd. (Tampere, Finland). Monolayer graphene on copper foil from Graphenea Inc. (San Sebastian, Spain) and transferred onto gold-coated SPR sensor chips using a PMMA-assisted wet transfer method adapted and modified from Reina et al. 2009 [65,66] (Fig. S1). The graphene/Cu foil was cut into smaller pieces using a rotary blade and fixed flat with Kapton tape to prevent curling. PMMA was spin-coated onto the graphene at 3000 rpm and baked at 120 °C for 3 min to ensure uniform coverage and good adhesion. The coated sample was treated with oxygen plasma for 35 s at 300 W to clean the surface and improve the subsequent copper etching. The film was then trimmed to match the dimensions of the SPR chips. Copper was etched in two steps: a short (~10 s) dip in a solution of 200 mL $H_2O$, 50 mL $H_2O_2$, and 50 mL of 37% HCl, followed by immersion in a second bath (600 mL $H_2O$, 50 mL $H_2O_2$, 50 mL HCl) for 20 min. The resulting PMMA/graphene film was transferred to deionized water and left for 24 h to improve cleanliness. The films were then lifted out using the SPR chips as substrates and left to dry under a laminar flow hood for an additional 24 h to ensure uniform adhesion and minimize wrinkles. Once dry, the chips were placed on a hot plate to reinforce bonding. The PMMA layer was subsequently removed in acetone, rinsed with isopropanol, and dried with a gentle stream of nitrogen. Quality of the transfer was assessed by optical microscopy, Raman spectroscopy with Renishaw plc (Wotton-under-Edge, UK) inVia 19 TM micro-Raman spectrometer with Green laser (532 nm) and 1800 grooves mm-1 (vis) gratings with a 50X magnification lens, and surface analysis, confirming a clean and intact graphene layer on the SPR chips (Figure S2, Figure S3).

All buffers were freshly filtered and degassed before the measurement. The SPR system MP-SPR Navi 210A VASA BioNavis Ltd. (Tampere, Finland) was primed with Tris-HCl buffer (pH 8, 50 mM). The sample was diluted in Tris-HCl buffer (pH 8, 50 mM) and injected over 20 min with a flow rate of 10 µL/min. Afterwards, the channel was washed for 20 min with Tris-HCl buffer (pH 8, 50 mM) with a flow rate of 10 µL/min. Signal detection was done with the 670 nm laser.

## 3. Results and discussion

The Fluoro4Graphene system was designed to provide a robust analytical screening platform for studying graphene binding that does not rely on additional biological agents, such as antibodies, for detection and does not require complex methods to prepare graphene surfaces,

such as vapor deposition. The developed screening is based on three steps (Fig. 1a) that only require standard laboratory equipment and can therefore be easily adopted by any biotechnologist or materials scientist, combining the two disciplines of materials science and protein engineering.

In the first step, the plate coating (I), a multilayered graphene surface is formed in a 96-well plate. In detail, a polytetrafluoroethylene (PTFE) filter plate was blocked with a bovine serum albumin (BSA)-containing buffer solution (5% (w/v)) overnight, which is needed to prevent unspecific protein binding during the Fluoro4Graphene assay. After blocking, the plate is coated with a freshly prepared graphene dispersion (1 mg/mL electrochemically exfoliated graphene in a dimethylformamide (DMF) suspension diluted in a 1:40 ratio with buffer solution) using vacuum filtration of the solution through the membrane. Afterwards, the plate is dried at 65 °C for 3 h to evaporate the remaining DMF; DMF removal ensures that neither the MBP binding nor the YmPh activity is affected. In the second step, the sample application (II), the MBP-YmPh fusions contained in the sample bind to the graphene surface. Purified protein or clarified *Escherichia coli* lysate, diluted in the BSA-containing buffer, can be used. In the third step, the signal detection (III), the amount of immobilized YmPh is determined by the detection of the fluorescence of the produced 4-MU ($\lambda_{ex/em}$ 372/445 nm; (Fig. 1b). Normalized fluorescence quantification can provide direct conclusions about the relative amount of protein on the graphene surface compared to a nonfunctionalized surface, or between different proteins. Only an indirect inference about the difference in binding strength under the defined measurement conditions can be drawn from this. The amount of protein per well (nmol/well) can be quantified by comparison to a standard reaction curve of the enzyme (see standard reaction curve; Fig. S4). A direct quantification of binding strength or affinity is not possible and, if necessary, requires further quantitative analytical methods following completion of the Fluoro4Graphen screening system. Fluorescence quenching by graphene is avoided by transferring the supernatant to a black 96-well microtiter plate.

### 3.1. Identification of suitable graphene-binding MBP

A diverse group of MBPs was selected and fused to YmPh to identify graphene-binding peptides for determining the robustness and reliability of the assay. The selected MBPs were Cecropin A (CeCa) (*Hyalophora cecropia*) (P01507) [68], Liquid Chromatography Peak I (LCI) (*Bacillus subtilis*) (P82243) [69], Macaque histatin 1 (MacHis) (*Macaca fascicularis*) (P34084) [56], Tachystatin A2 (TA2) (*Tachypleus tridentatus*) (Q9U8X3) [70], and a known carbon-binding peptide (CBP1) [43]. Their binding to graphene was analyzed from clarified lysate via the developed assay (Fig. 2). Based on the high number of aromatic amino acids, which should bind via π-π stacking to the graphene, we expected MacHis and CBP1 to be retained comparatively high on the graphene surface. As expected, MacHis showed the highest fluorescence signal, but surprisingly, CBP1 did not show any signal. Previously, the binding properties of CBP1 were investigated on planar surfaces or single-walled carbon nanotubes, differing from the surface used in this system [43, 71–74]. Additionally, the reported peptide was mainly characterized without a fusion protein attached, in contrast to the method presented here [43]. Enhanced GFP (eGFP) fusion via an ELISA-based approach was tested to ensure the lower binding was not caused by the phytase fusion, which showed only weak binding for CBP1 as well. (Fig. S5).

Based on the results obtained for the MacHis fusion proteins with YmPh and eGFP, MacHis was identified as a suitable graphene-binding peptide and used in all subsequent measurements to develop and validate the Fluoro4Graphene screening system.

### 3.2. Robustness of the Fluoro4Graphene screening system

For the development of a high-throughput applicable screening assay, the coefficient of variation (CV) is a critical parameter, as it defines the lower limit of performance improvements that can be reliably detected. If the CV is too high, experimental noise and signal fluctuations obscure small improvements, which is particularly problematic when baseline binding levels are already substantial, and further enhancement is inherently limited by complete surface coverage. Consequently, the CV is a key metric for evaluating the suitability of

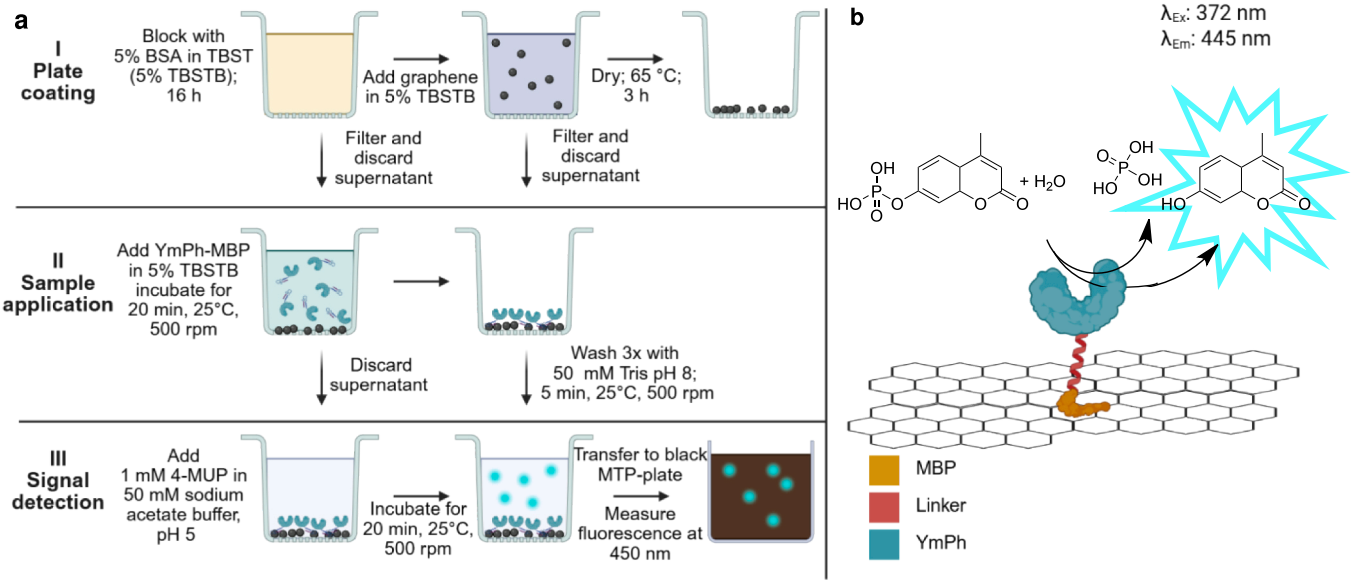


**Fig. 1. Workflow of the Fluoro4Graphene system for the detection of protein binding to graphene.** (a) The Fluoro4Graphene system is divided into three steps. First, filter plates are coated (I), starting by blocking the surface against unspecific binding. Later, a graphene dispersion is used to generate a graphene-coated surface. For the sample application (II), bifunctional proteins are added to the microtiter plate. After binding, the unspecifically bound protein gets washed away in three washing steps. For signal detection (III), the surrogate substrate for YmPh, 4-MUP, is added. The product is quantified by fluorescence detection after transfer to a fresh microtiter plate. (b) Immobilized bifunctional proteins containing the binding domain (MBP), a rigid linker as a spacer and the phytase on the graphene-coated surface of the microtiter plate, reacting with 4-MUP to produce fluorescent 4-MU. Parts of the figure were created with BioRender [67].

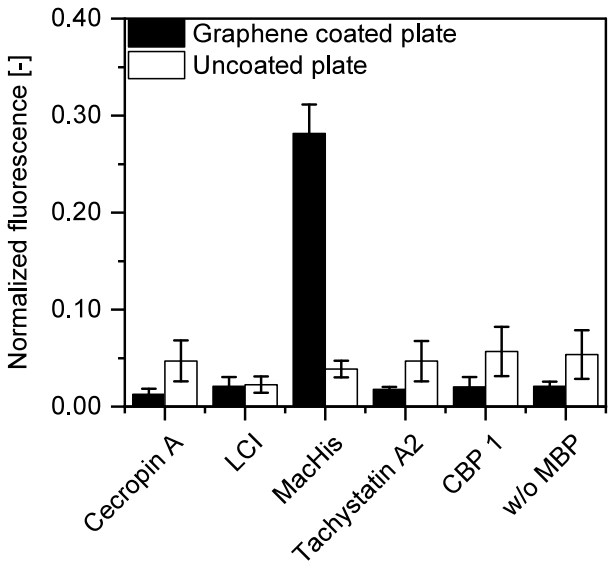


**Fig. 2. Fluorescent binding signal of different MBPs using the Fluoro4Graphene system.** Comparison of protein binding on graphene amongst various peptides fused to YmPh. Bacteria were cultured in 96-well microtiter plates. Diluted lysate (3:7) of the cell pellet was used for protein immobilization. w/o MBP relates to a control expressing only the YmPh phytase without a genetically fused peptide. Samples bound to the graphene-coated surface (■) were compared to samples bound to an uncoated control plate (□). The signal was normalized to the signal of the crude lysate. Mean and standard deviation were calculated from three biological replicates.

screening methods for directed evolution campaigns. High-throughput screenings provide a fast overview of large sample sizes, usually followed by validation of individual variants using highly sensitive and established analytical methods. A CV of <20% is within an acceptable and comparable range for these systems, especially in the field of biotechnology [58,59]. Here, accuracy can be affected not only by technical error sources but also by expression levels or lysis differences across single biological replicates or variants [58,59]. Therefore, a lower CV is not required as long as the fluctuation does not impede the identification of improved binders.

The underlying 4-methylumbelliferyl phosphate (4-MUP)-based detection chemistry is well established and was therefore not substantially modified [75]; only the complexity and concentration of the sodium acetate buffer were reduced to decrease buffer-induced background signal and increase the YmPh activity (Fig. S6a).

The optimal lysate volume for achieving a favorable signal-to-background ratio was determined by testing lysate volumes from 10 to 150 µL for binding to graphene. All tested volumes were within the linear range (Fig. 3a), and the background-to-signal ratio decreased as lysate volume increased. For consistent signal quantification within the linear range, 75 µL of lysate was used per well during high-throughput screening in a 96-well format.

To assess assay variability under realistic screening conditions, a full 96-well plate of MacHis wild type (WT)-YmPh biological replicates was produced, lysed, clarified, and the YmPh activity was measured. The lysate was then transferred to the graphene-coated plate, and the assay was performed as described above. Signal fluctuations caused by variations in expression and cell lysis efficiency were minimized by normalizing with the previously measured signal of the corresponding clarified lysate for all subsequent measurements. The observed normalized signal strength exhibited an apparent coefficient variance (CV) of 16.6% and a background-corrected ("true") CV of 17.9%, accounting for nonspecific binding to uncoated plates (Fig. 3b). In a detailed investigation to further dissect the origin of assay variability, the technical error of the Fluoro4Graphene system was measured. Two full plates, a graphene-coated plate and an uncoated plate, with technical replicates, were compared. Yielding CVs of 14% for the graphene-coated plate and 3% for the uncoated plate (Fig. 3c), indicating that the dominant source of variability originates from the graphene coating rather than from the fluorogenic detection or liquid handling. These results demonstrate that normalization effectively compensates for biological variability. In contrast, the technical variability results in a comparable degree of heterogeneity on the non-planar filter surface formed by electrochemically exfoliated graphene flakes, thereby building a multilayered graphene surface. Therefore, the Fluoreo4Graphene system can be used as a fast and practical method for identifying individual proteins or variants. If more information on the quantification of binding strength is required, these proteins should always be investigated further using more surface-sensitive, quantitative methods on a high-quality graphene monolayer.

The stability of pre-coated graphene plates was evaluated by storing a coated plate at 4 °C for seven days and comparing its performance with that of a freshly prepared plate. No loss in fluorescence signal was observed for the stored plate, and only a minor increase in deviation was detected (Fig. 3d). In subsequent experiments with additional MBP variants, this increased deviation was no longer observed, indicating that the coating and blocking procedures yield stable and reproducible surfaces (Fig. S6b).

Finally, the applicability of the screening method across different pH conditions was assessed by washing in buffers ranging from pH 8 (Tris) to pH 5 (sodium acetate), which correspond to the assay buffers. After protein binding, washing could be performed with either buffer without affecting signal intensity. The YmPh-MacHis fusion remained bound at lower pH values, and YmPh activity was retained (Fig. 3e), consistent with the reported robustness of the enzyme across a broad range of conditions [75].

In summary, the broad linear range, low CV, and robustness to storage and varying buffer conditions position the Fluor4Graph screening system as a promising high-throughput screening method for the directed evolution of MBPs for graphene.

### 3.3. *Validation of Fluoro4Graphene screening system by directed evolution of YmPh-MacHis for improved binding to graphene*

A directed evolution campaign for MacHis was conducted to validate the system. In total, 840 YmPh-MacHis variants were screened. The error-prone PCR (epPCR) to generate mutations (DNA level) was only applied to the MBP MacHis coding region. An $MnCl_2$ concentration of 0.3 mM resulted in a mutational frequency of 12 per kilobase, yielding 1.4 mutations on average in the MacHis gene. The Fluoro4Graphene system showed a high fluorescent signal of the MacHis fusion proteins to the surface, while SPR measurements determined a surface coverage of about 106 ng/cm$^2$ of YmPh-MacHis (Fig. 6b). The approximate surface coverage was calculated (Table S3) using an AlphaFold model of the protein to estimate its size and shape (Fig. S7). Assuming a monolayer on a planar surface, the approximate surface coverage should be 54%, allowing for roughly a twofold improvement in binding. Therefore, all variants with an improvement of more than 1.5 in the first screening round were rescreened. The eleven best-performing variants were subsequently sequenced (Fig. 4).

In the 11 best-performing variants, the following exchanges were observed: Five substitutions from glutamic acid (negative charge) to other uncharged amino acids, primarily glycine. Five substitutions from histidine to arginine (positive charge). Two truncations that removed aspartic acid (negative charge). Overall, these alterations reduce the number of negative charges, resulting in a peptide with a net charge of +4 to +5 instead of +3. Two types of substitutions were observed here: the introduction of positive charges by arginine or the reduction of negative charges by exchange or removal of negatively charged amino acids (Fig. 4a) [76].

Previous studies showed that mainly aromatic and positively

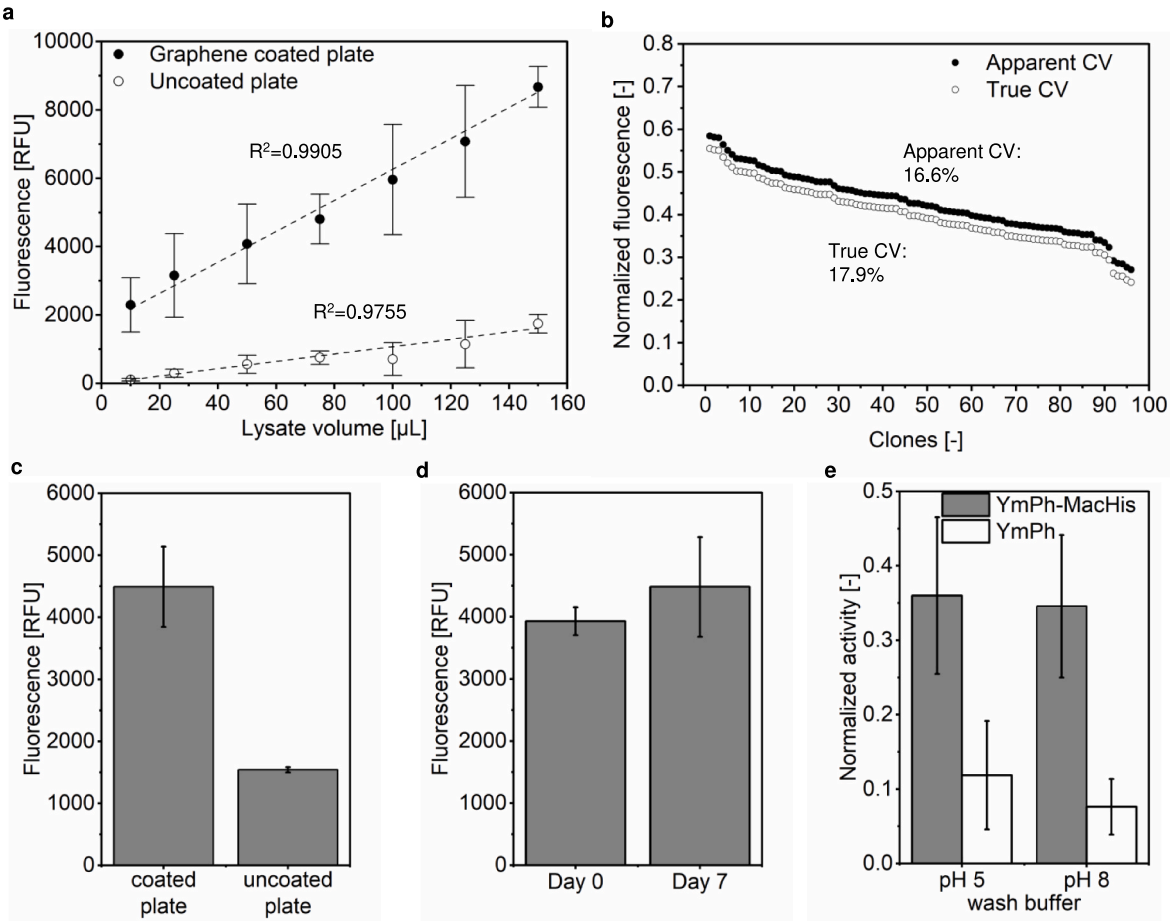


**Fig. 3. Validation of the Fluoro4Graphene system as a high-throughput screening system.** (a) Linear correlation between lysate volumes from 10 to 150 µL and fluorescence signal for YmPh-MacHis bound to a graphene-coated plate (●) and an uncoated plate (○). Mean and standard deviation were calculated from 42 biological replicates for each condition. The coefficient of determination ($R^2$) was calculated with OriginPro 2024. (b) Apparent coefficient of variation (CV) (●) and true CV (○) after subtraction of the background signal. The signal of bound protein was normalized against the fluorescence signal of the crude lysate. Apparent CV was measured in 96 biological replicates of protein bound to a graphene-coated plate. Background signal was measured in 96 biological replicates of protein bound to an uncoated plate. (c) Binding test of technical replicates for the detection of technical error. *E. coli* BL21 (DE3) $lacI^{Q1}$ harboring the overexpression plasmid encoding ymph-machis WT was incubated (8 h, 37 °C, 200 rpm) in LB medium containing 50 µg/mL carbenicillin. The culture was diluted 1:100 in 200 mL ZYM-medium, and protein was produced for 16 h, 37 °C, 200 rpm shaking. Bacteria were centrifuged (8000 rpm, 10 min, 4 °C, Sorvall). The pellet was resuspended in 10 mL 5% BSA in TBST (50 mM Tris-HCl pH 8, 150 mM NaCl, 0.05% Tween). The bacterial cells were lysed with 15 mg/mL lysosome, and the cell debris were centrifuged for 30 min, 4 °C at 4000 rpm. The supernatant was used for the Fluoro4Graphene system with a whole 96-well microtiter plate coated with graphene and an uncoated 96-well microtiter plate (175 µL 5% BSA TBST + 75 µL lysate per well). Mean and standard deviation were calculated from 96 technical replicates. (d) Minimal possible storage time for graphene-coated plates. Two 96-well PTFE microtiter filter plates were blocked with 5% TBSTB overnight and coated with 100 µL of 20 ng/mL graphene in 5% BSA TBST. One plate was stored at 4 °C for 7 days, and the other was prepared fresh on the day of the experiment. 200 nM of purified YmPh-MacHis was added in 4 technical replicates. The Fluoro4Graphene system was conducted on both plates in parallel. Means and standard deviation were calculated from four technical replicates. (e) Stability tests of immobilized YmPh on graphene-coated filter plates. 48 biological replicates of each, YmPh-MacHis and YmPh without an MPB, were immobilized on a graphene-coated plate as negative controls. After immobilization, 24 replicates of each protein were washed with 50 mM sodium acetate buffer (50 mM, pH 5), and 24 replicates were washed with Tris-HCl (50 mM, pH 8). The further Fluoro4Graphene system was conducted as usual.

charged amino acids are beneficial for binding to graphene [28–30,77]. Arginine was previously identified several times as one of the best binders [28–30,77]. Interestingly, almost no exchanges to the positively charged amino acid lysine were found. Although lysine can be absorbed onto the graphene surface due to electrostatic cation-π interactions over the amine group ($NH_3^+$). Previous reports suggest that the long alkyl chain leads to steric hindrance as well as a higher energetic penalty during adsorption due to the stronger hydration shell formed by the localized charge at the amine group. On the other hand, the guanidinium moiety of arginine is planar with a delocalized charge, leading to a smaller hydration shell and adding the possibility to bind via π-π stacking due to its $sp^2$ hybridized carbon to graphene surfaces in addition to electrostatic interactions [28,78,79]. This leads to a low free energy of adsorption, making arginine a favorable binder [28]. The strong binding of arginine to graphene is also in agreement with our measurement. Here, arginine is preferred over histidine. The imidazole ring of histidine can be positively charged under acidic conditions, thereby enhancing binding to graphene via electrostatic interactions. Under neutral conditions, histidine can only interact via π-π stacking. Simulations showed that arginine binding is energetically preferred at neutral pH, likely due to the planar moiety and the combined cation-π and π-π interactions [31,80]. Besides the introduction of positive charges, the reduction of negative charges was observed. In two variants, the peptide was truncated at the C-terminus by exchanging tyrosine for a stop codon, resulting in the deletion of an aspartic acid. Negatively charged amino acids have a high free energy of adsorption due to their repulsive net charge, as well as their hydrophilic nature, and are therefore unfavorable for binding to graphene [28]. The second trend observed for the reduction of negative charge was the exchange of glutamate at position 4. Here, 80% of the substitutions were towards

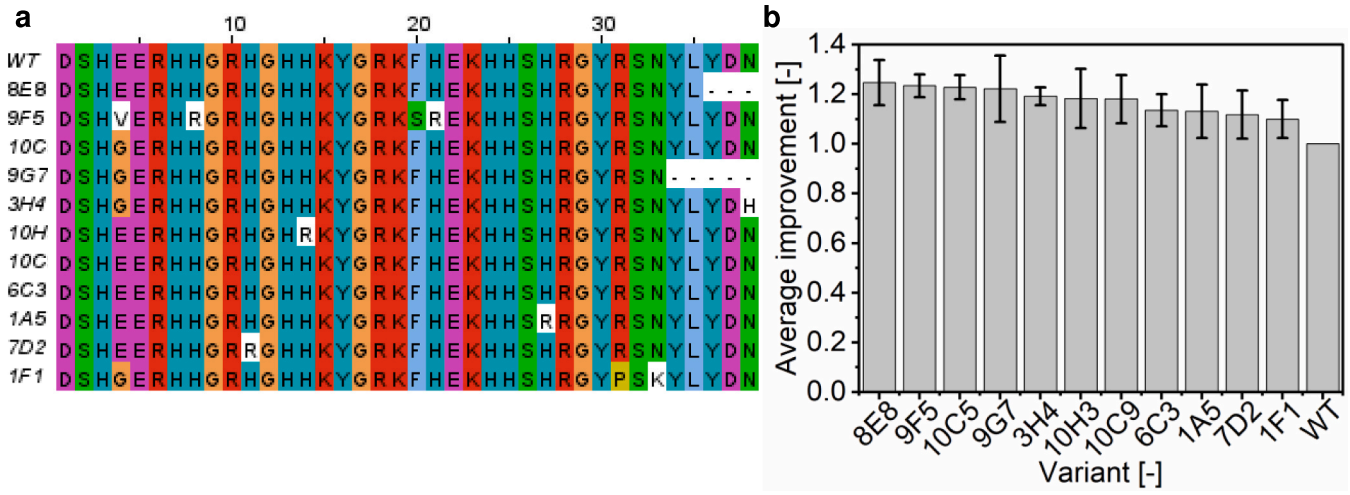


**Fig. 4. Screening of improved variants YmPh-MacHis.** (a) Multiple sequence alignment of the MacHis wild type sequence compared to the sequences of the 11 best-performing YmPh-MacHis variants. Illustration done by Jalview. [76]. (b) Normalized 4-MU fluorescence values of the 11 selected YmPh-MacHis variants compared to the wild-type YmPh-MacHis from clarified lysate. The mean of three biological replicates of each variant was normalized against the mean of three biological replicates of the wild type. The experiment was replicated three times in total, and the mean and standard deviation were calculated from these 9 replicates in total.

glycine. In addition to the peptide's interaction with the graphene surface, its interaction with the water layer above the surface should be considered. Compact amino acids, such as glycine, cause less unfavorable interactions between the bound peptide and the dense water layer above the graphene surface [28]. Similarly, the beneficial binding of positively charged amino acids, especially arginine, to hydrophobic surfaces has been reported several times, leading to the suggestion that they create more favorable interfaces between water and the material [81–83]. Arginine's amphiphilic character, arising from the guanidinium group, allows hydrophobic interaction with the graphene surface while still creating a favorable interface with water through its charge [84].

As general trends in preferred protein binding to the graphene surface, low free energy of adsorption due to positive charge/cation-π interaction, π-π stacking, and hydration energy, as well as the compactness of amino acids, were observed. Therefore, one variant, 10H3 with an introduced arginine (H14R), and one variant, 10C5 with an introduced compact amino acid (E4G), were chosen for in-depth characterization.

### 3.4. Biophysical characterization of YmPh-MacHis binding on graphene

In detail, the biophysical characterization of purified protein fractions from the wild type and the variants E4G and 10H3 (Figs. S6 and S8) was performed to determine the dependency of binding on pH and salt concentrations and to assess the feasibility of the assay within these working ranges. When considering pH dependency, the wildtype exhibits a binding optimum between pH 7 and 8 (Fig. 5a). The exchange of glutamic acid for glycine in variant 10C5 led to an overall improvement in binding above pH 4, with an enhanced plateau in the alkaline region between pH 9 and 10. In the wild type, glutamic acid develops a repulsive net negative charge above its p$K_R$ of 4.25 [86], resulting in a decreasing hydration energy. This makes the transition from the aqueous solution to the hydrophobic graphene surface energetically unfavorable at pH values above 4. When considering the net charge of the wild type and the variant, it is notable that the variant has a generally higher net charge, especially at pH > 7, with over +1 (Table S4), suggesting mostly electrostatic effects influencing the increased binding in the alkaline milieu of variant 10C5. In addition, as discussed in chapter 3.3, steric reasons and a smaller hydration shell can lead to decreased adsorption energy [28]. In the variant 10H3, the

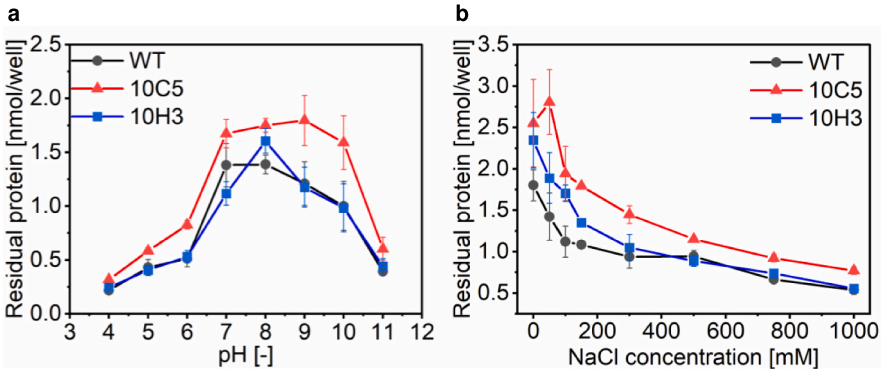


**Fig. 5. Binding dependency of YmPh-MacHis** WT (●), 10C5 (▲), and 10H3 (■) on pH (a) and NaCl concentration (b). Bound, purified protein with an initial concentration of 200 nM was detected by the Fluoro4Graphene system with different pH (Citrate buffer 50 mM pH, 4, 5, 6; Tris HCl Buffer 50 mM pH 7, 8, 9; CAPS buffer 50 mM 10, 11) (a) or NaCl concentrations (0, 50, 100, 150, 200, 300, 500, 750, 1000 mM) (b) in the washing buffer. Residual protein concentrations in the well were determined using a standard reaction curve with a correlation between protein concentration and fluorescence signal. Mean and standard error of the mean were calculated from four (a) or three (b) biological replicates.

exchange of histidine for arginine led to a narrower but improved performance optimum, occurring only at pH 8. In an acidic environment under pH 7 and in an alkaline environment over pH 8, both peptides behave the same. This suggests a smaller electrostatic effect, with π-π stacking instead stabilized, probably due to steric or hydrophobic interactions [28,78].

The assay performance over the whole pH range suggests that the acidic phytase is active independent of pH pretreatment [87] during the washing steps and yields reliable results for quantifying the retained protein on the surface under all conditions.

The dependency on salt and ionic strength showed decreased residual protein with increased NaCl concentrations for the wildtype as well as both variants (Fig. 5b). For NaCl concentrations ranging from 0 to 150 mM, both variants exhibited improved binding capacity compared to the wild type. At NaCl concentrations above physiological conditions, only variant 10C5 showed an improved signal, while the signal for 10H3 was consistent with the wild type. Again, for variant 10C5, the removal of electrostatic repulsion and the decrease in local hydration energy led to a small overall improvement that is effective regardless of ionic shielding [28,88]. In the variant 10H3, the positively charged guanidinium group is outperforming the uncharged histidine chain at lower salt concentrations due to the above-discussed charge-driven and cation-π interactions, with low competition with the $Na^+$ ions. At NaCl concentrationsabove the physiological range, an ion atmosphere can screen the charges of the peptide, weakening long-range electrostatic attraction and thereby inhibiting both variants by forming an ion shield around the side chains, leading to decreased protein-surface interaction equally [89,90]. On the other hand, high ion concentrations are known to influence the interfacial water structure at graphene surfaces and interfere with the formed water double layer over graphene [91–93]. These observations on the wildtype and both variants suggest that higher salt concentrations over 150 mM have not only an influence on the variants but might have a general effect on protein binding to graphene due to ion shielding and interface stabilization of protein-water and graphene-water, leading to a general impairment of the assay, not being able to discriminate improved protein binding any longer.

Overall, the assay can be used in a working range at pH 4 to 11, with the phytase remaining active as a reporter, independent of pretreatment. Regarding ionic strength, low salt concentrations up to 150 mM are recommended to enable measurement of protein binding with minimal deviation from physiological conditions. The observed sequence trends for protein binding at pH 8 in the absence of salt can be extrapolated to a broader set of pH and salt concentrations for variant 10C5, but not for 10H3. Therefore, not all variants identified by this assay can be classified as general better graphene binders. The identification of improved binders always depends on the chosen screening conditions [94] and can be adapted in the washing step when screening for better graphene binders for specific applications.

In addition, the influence of the graphene surface, which utilizes a multilayered microtiter plate scaled graphene surface formed from electrochemical graphene flakes used in this assay, compared with high-quality monolayer graphene, cannot be excluded. The screening platform offers a fast easy-to-use approach for high-throughput screening that needs subsequent validation using established surface-sensitive methods. Therefore, changes of the relative surface retention detected by the Fluoro4Graphene platform were compared to SPR measurements of surface mass, using a transferred monolayer of CVD graphene on gold chips [85]. Among AFM, QCM-D, and SPR, SPR was chosen as a single, low-throughput but sensitive, straightforward, and direct quantitative method to validate the robustness of the Fluoro4Graphene platform.

The relative surface retention of both variants, E4G and 10H3, and the wild type was tested using the Fluoro4Graphene system at initial protein concentrations ranging from 100 to 600 nM after purification. The determined reaction curve for each variant was used to quantify the remaining protein on the surface (Figure S4, Fig. 6a). The reaction curve, measured with purified, free protein in a 1:30 dilution of protein concentrations ranging from 0 to 1000 nM in solution, showed a linear range from 0 to approximately 15 nM, yielding a lower limit of quantification directly above 0 nM. With this, the Fluoro4Graphene system provides a sensitive analytical method for low concentrations of protein. The single mutation variants showed higher binding compared to the wild type with a significant increased amount of bound protein: 10C5 was 1.35 times improved (4.50 nmol/well) at 200 nM of initial protein concentration, while 10H3 was 1.45 improved (4.83 nmol/well) at 200 nM and 1.21 times improved (4.97 nM/well) at 300 nM of initial protein concentration (Fig. 6b). At initial concentrations higher than 400 nM, the recorded 4-MU signal reached a plateau, around 4.5 nmol/well for the wild type and 5 nmol/well for both variants. The Fluro4Graphene screening system has a linear detection range for YmPh-MacHis fusion proteins in the initial protein concentration range of 100 to 400 nM. The latter would be a good starting point to investigate other YmPh-MBP fusions.

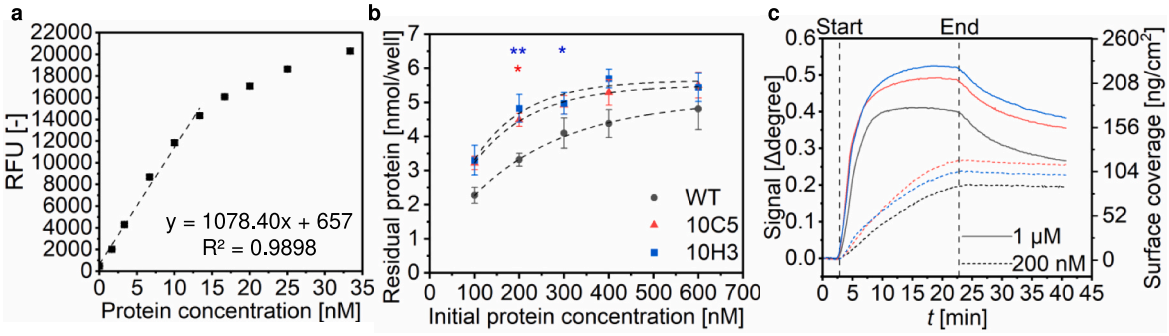


**Fig. 6. Characterization of improved variants** YmPh-MacHis 10C5 (▲) and 10H3 (■) compared to the wild type (●). (a) Standard reaction curves for the quantification of YmPh-MacHis WT with the Fluoro4Graphene system. 5 µL of different concentrations (50, 100, 200, 300, 400, 500, 600, 750 and 1000 nM) of purified protein were diluted with 145 µL of 1 mM 4-MUP in 50 mM sodium acetate buffer in a black microtiter plate. The plate was incubated for 20 min, 25 °C, 200 rpm shaking, then fluorescence was measured $\lambda_{Ex/EM}$: 360-20/50-30. Mean and standard deviation were measured in technical triplicate. The regression curve was calculated with Microsoft Excel 2019 within the linear range (–). For every purification, a new standard was measured. The graphs and equations shown above are representative (b) Bound, purified protein detected by Fluoro4Graphene system with different initial protein concentrations. The background signal of the buffer in the plate was subtracted from the signal. Residual protein concentrations in the well were determined using a standard reaction curve with a correlation between protein concentration and fluorescence signal. Mean and standard error of the mean were calculated from five biological replicates. Curve fitting and statistical analysis were calculated with OriginPro 2024 using the one-phase exponential decay function and ordinary paired *t*-test: *p < 0.05, **p < 0.01 (c) SPR characterization of the variants and the wild type with 1 µM (–) and 200 nM (---) protein concentration. All proteins were diluted in Tris-HCl buffer (50 mM, pH 8) and injected for 20 min with a flow rate of 10 µL/min. Post injection, all channels were washed for 20 min with Tris-HCl buffer (50 mM, pH 8) with a flow rate of 10 µL/min. The conversion from the signal output Δdegree of the MP-SPR Navi 210A VASA to ng/cm$^2$ was calculated according to Söder et al. [85].

SPR with monolayered high-purity chemical vapor deposited (CVD) graphene was performed to validate the results of the Fluoro4Graphene system. The surface coverage of the wild type and both variants, E4G and 10H3, was determined with two initial protein concentrations: one within the linear range of the Fluoro4Graphene system (200 nM) and a second above this range (1 μM). The SPR measurements showed improved binding for both variants at both concentrations compared to the wild type, verifying the results gained with the Fluoro4Graphene system (Fig. 6c). At 1 μM of initial protein concentration, the surface coverage increased from 106.19 ng/cm$^2$ to 144.17 ng/cm$^2$ for the variant 10C5 and to 154.10 ng/cm$^2$ for 10H3 (Table S5). These changes translate to relative improvements of 1.35 for 10C5 and 1.44 for 10H3, mirroring the values determined with the Fluoro4Graphene system. The shift from a large-scale multilayered graphene surface formed by electrochemically exfoliated graphene flakes in microtiter plate format to a monolayer of CVD graphene transferred to the SPR chip did not influence the relative change in binding for the tested variants. Although the evaluation of only two variants on these two graphene materials is insufficient to generalize this observation to all proteins that can be identified by the Fluoro4Graphene platform, the results provide a promising indication of the platform's transferability between different graphene surfaces. These findings further support that the Fluoro4Graphene system provides quantitatively reliable results, making it suitable for identifying improved binders in large lab-scale directed evolution campaigns of MBPs for graphene binding. Improved MBPs, in the range of 1.3 to 1.5 times improvement, can enhance the performance of biointerfaces, for instance, in biosensing applications, by increasing signal intensity and sensitivity through higher surface coverage, as well as by improving system robustness via reduced desorption under varying process conditions [95,96].

## 4. Conclusion

The fluorogenic high-throughput screening platform Fluoro4Graphene enables the quantitative evaluation of graphene-binding peptides and proteins for defined screening conditions. The method does not rely on vapor deposition or other complex instrumentation and can therefore be readily implemented in standard laboratory environments. Importantly, samples can be analyzed directly from *E. coli* lysates without purification, substantially simplifying the workflow and increasing throughput.

The performance of Fluoro4Graphene was validated in a first directed evolution campaign of YmPh-MacHis comprising 840 variants. This screening identified the improved variant YmPh-MacHis H14R, whose enhanced graphene binding was independently confirmed by surface plasmon resonance. The graphene surface coverage increased from 106 ng /cm$^2$ to 154 ng /cm$^2$. In addition, the assay reliably resolved sequence-dependent binding trends, with improved variants showing an increased number of positively charged residues and a reduced number of negatively charged residues.

Overall, the platform combines high throughput, robustness, and compatibility with microtiter plate formats, making it well-suited for systematic screening and comparative analysis of graphene-binding biomolecules. Fluoro4Graphene thus represents a versatile analytical methodology for studying and engineering biofunctional graphene interfaces and may facilitate the development of reproducible, scalable, and cost-effective graphene functionalization strategies from aqueous solutions.

## Novelty statement

This study presents Fluoro4Graphene, a fluorogenic high-throughput analytical assay for the quantitative assessment of protein-graphene interactions. By decoupling signal generation from the graphene surface through an enzyme-mediated solution-phase readout, the method overcomes fluorescence quenching and enables reproducible, quantitative measurements directly from crude cell lysates. The platform is analytically validated through independent SPR measurements and demonstrated in a directed evolution workflow, enabling the resolution of minimal sequence-dependent binding differences.

## Declaration of generative AI and AI-assisted technologies in the manuscript preparation process

During the preparation of this work, Grammarly (Grammarly Inc.) was used for natural language processing tasks to perform light editing of the original text, such as correcting grammar or spelling. After using this tool, the authors reviewed and edited the content as needed. They take full responsibility for the content of the publication.

## CRediT authorship contribution statement

**Ines Vogt:** Conceptualization, Data curation, Formal analysis, Investigation, Methodology, Validation, Visualization, Writing – original draft. **Florian Bourdeaux:** Conceptualization, Methodology, Project administration, Writing – review & editing. **Tetiana Kurkina:** Methodology, Project administration, Writing – review & editing. **Aidin Nikookhesal:** Resources, Visualization, Writing – original draft. **Sven Ingebrandt:** Funding acquisition, Resources, Supervision, Writing – review & editing. **Vivek Pachauri:** Conceptualization, Resources, Writing – review & editing. **Ulrich Schwaneberg:** Conceptualization, Funding acquisition, Methodology, Project administration, Supervision, Writing – review & editing.

## Declaration of competing interest

The authors declare that they have no known competing financial interests or personal relationships that could have appeared to influence the work reported in this paper.

## Acknowledgements

Parts of Fig. 1 (https://BioRender.com/0yvq7ju) and the graphical abstract (https://BioRender.com/aq6s06c) were created with BioRender.com. Microfabrication was carried out in the Central Laboratory for Micro- and Nanotechnology (CMNT) at RWTH Aachen University. Technical support by CMNT staff is gratefully acknowledged. We thank the Federal Ministry of Research, Technology and Space (BMFTR) former Federal Ministry of Education and Research (BMBF) for funding our study via BÖR_BioTech Innovationslabor ProtLab (FKZ: 031B1134C). We acknowledge the funding of the Federal Ministry of Research, Technology and Space (BMFTR) former Federal Ministry of Education and Research (BMBF) and the Ministry of Culture and Science of the German State of North Rhine-Westphalia (MKW) under the Excellence Strategy of the Federal Government and the Länder via the project Pep2D (Projekt-ID G:(DE-82)EXS–SF–BioTrans013).

## Appendix A. Supplementary data

Supplementary data to this article can be found online at https://doi.org/10.1016/j.talanta.2026.130063.

## Data availability

Data will be made available on request.

## References

[1] A.N. Banerjee, Graphene and its derivatives as biomedical materials: future prospects and challenges, Interface Focus 8 (2018) 20170056.
[2] S. Kumar, S.H. Parekh, Linking graphene-based material physicochemical properties with molecular adsorption, structure and cell fate, Commun. Chem. 3 (2020) 8.

[3] P. Hampitak, D. Melendrez, M. Iliut, M. Fresquet, N. Parsons, B. Spencer, T. A. Jowitt, A. Vijayaraghavan, Protein interactions and conformations on graphene-based materials mapped using a quartz-crystal microbalance with dissipation monitoring (QCM-D), Carbon 165 (2020) 317–327.

[4] E.D. Sitsanidis, J. Schirmer, A. Lampinen, K.K. Mentel, V.-M. Hiltunen, V. Ruokolainen, A. Johansson, P. Myllyperkiö, M. Nissinen, M. Pettersson, Tuning protein adsorption on graphene surfaces via laser-induced oxidation, Nanoscale Adv. 3 (2021) 2065–2074.

[5] E.N. Primo, S. Bollo, M.D. Rubianes, G.A. Rivas, Immobilization of graphene-derived materials at gold surfaces: towards a rational design of protein-based platforms for electrochemical and plasmonic applications, Electrochim. Acta 259 (2018) 723–732.

[6] A. Kasry, A.A. Ardakani, G.S. Tulevski, B. Menges, M. Copel, L. Vyklicky, Highly efficient fluorescence quenching with graphene, J. Phys. Chem. C 116 (2012) 2858–2862.

[7] S. Dedisch, A. Wiens, M.D. Davari, D. Söder, C. Rodriguez-Emmenegger, F. Jakob, U. Schwaneberg, Matter-tag: a universal immobilization platform for enzymes on polymers, metals, and silicon-based materials, Biotechnol. Bioeng. 117 (2020) 49–61.

[8] C. Zumpe, C.L. Bachmann, A.U. Metzger, N. Wiedemann, Comparison of potency assays using different read-out systems and their suitability for quality control, J. Immunol. Methods 360 (2010) 129–140.

[9] L.-H. Tran, C. Lee, T.J. Kang, S.-H. Jang, Graphene oxide-mediated fluorescence quenching of green fluorescent protein for biomedical applications, Bulletin Korean Chem Soc 37 (2016) 1265–1269.

[10] D.G. Papageorgiou, I.A. Kinloch, R.J. Young, Mechanical properties of graphene and graphene-based nanocomposites, Prog. Mater. Sci. 90 (2017) 75–127.

[11] S. Szunerits, R. Boukherroub, Graphene-based biosensors, Interface Focus 8 (2018) 20160132.

[12] C. Liao, Y. Li, S.C. Tjong, Graphene nanomaterials: synthesis, biocompatibility, and cytotoxicity, Int. J. Mol. Sci. 19 (2018).

[13] Rasu Ramachandran, Veerappan Mani, Shen-Ming Chen, Ramiah Saraswathi, Bih-Show Lou, Recent trends in graphene based electrode materials for energy storage devices and sensors applications, Int. J. Electrochem. Sci. 8 (2013) 11680–11694.

[14] A.M. Narváez-Romero, F.J. Rodríguez-Lozano, M.P. Pecci-Lloret, Graphene-Based materials for bone regeneration in dentistry: a systematic review of In vitro applications and material comparisons, Nanomaterials 15 (2025).

[15] J. Lin, X. Chen, P. Huang, Graphene-based nanomaterials for bioimaging, Adv. Drug Deliv. Rev. 105 (2016) 242–254.

[16] S. Song, H. Shen, Y. Wang, X. Chu, J. Xie, N. Zhou, J. Shen, Biomedical application of graphene: from drug delivery, tumor therapy, to theranostics, Colloids and surfaces. B, Biointerfaces 185 (2020) 110596.

[17] K. Yang, S. Zhang, G. Zhang, X. Sun, S.-T. Lee, Z. Liu, Graphene in mice: ultrahigh in vivo tumor uptake and efficient photothermal therapy, Nano Lett. 10 (2010) 3318–3323.

[18] J. Peña-Bahamonde, H.N. Nguyen, S.K. Fanourakis, D.F. Rodrigues, Recent advances in graphene-based biosensor technology with applications in life sciences, J. Nanobiotechnol. 16 (2018) 75.

[19] G. Khutale, S. Andhari, R. Gupta, G. Aland, S. Banerjee, K. Todkar, M. Pore, V. Khobragade, A. D'Souza, N. Kale, A. Vasudevan, A. Bharde, S. Jayant, Y. Patil, J. Khandare, A multicomponent nanosystem for capturing circulating tumor cells from cancer patients with PD-L1 as an immunotherapy oncotarget, J. Mater. Chem. B 12 (2024) 10973–10982.

[20] S. Sattari, M. Adeli, S. Beyranvand, M. Nemati, Functionalized graphene platforms for anticancer drug delivery, International journal of nanomedicine 16 (2021) 5955–5980.

[21] S. Joshi, P. Sharma, R. Siddiqui, K. Kaushal, S. Sharma, G. Verma, A. Saini, A review on peptide functionalized graphene derivatives as nanotools for biosensing, Mikrochim. Acta 187 (2019) 27.

[22] V. Georgakilas, M. Otyepka, A.B. Bourlinos, V. Chandra, N. Kim, K.C. Kemp, P. Hobza, R. Zboril, K.S. Kim, Functionalization of graphene: covalent and non-covalent approaches, derivatives and applications, Chemical reviews 112 (2012) 6156–6214.

[23] D. Saini, Synthesis and functionalization of graphene and application in electrochemical biosensing, Nanotechnol. Rev. 5 (2016).

[24] Z. Jin, J.R. Lomeda, B.K. Price, W. Lu, Y. Zhu, J.M. Tour, Mechanically assisted exfoliation and functionalization of thermally converted graphene sheets, Chem. Mater. 21 (2009) 3045–3047.

[25] X. Zhang, L. Hou, A. Cnossen, A.C. Coleman, O. Ivashenko, P. Rudolf, B.J. van Wees, W.R. Browne, B.L. Feringa, One-pot functionalization of graphene with porphyrin through cycloaddition reactions, Chemistry (Weinheim an der Bergstrasse, Germany) 17 (2011) 8957–8964.

[26] V. Georgakilas, J.N. Tiwari, K.C. Kemp, J.A. Perman, A.B. Bourlinos, K.S. Kim, R. Zboril, Noncovalent functionalization of graphene and graphene oxide for energy materials, biosensing, catalytic, and biomedical applications, Chemical reviews 116 (2016) 5464–5519.

[27] M. Matiyani, M. Pathak, B.S. Bohra, N.G. Sahoo, Noncovalent functionalization of carbon nanotubes, in: J. Abraham, S. Thomas, N. Kalarikkal (Eds.), Handbook of Carbon Nanotubes, Springer International Publishing, Cham, 2022, pp. 421–448.

[28] Z.E. Hughes, T.R. Walsh, What makes a good graphene-binding peptide? Adsorption of amino acids and peptides at aqueous graphene interfaces, Journal of materials chemistry B 3 (2015) 3211–3221.

[29] A.N. Camden, S.A. Barr, R.J. Berry, Simulations of peptide-graphene interactions in explicit water, The journal of physical chemistry. B 117 (2013) 10691–10697.

[30] N. Dragneva, W.B. Floriano, D. Stauffer, R.C. Mawhinney, G. Fanchini, O. Rubel, Favorable adsorption of capped amino acids on graphene substrate driven by desolvation effect, The Journal of chemical physics 139 (2013) 174711.

[31] W. Luo, C. Homma, Y. Hayamizu, Rational design and self-assembly of histidine-rich peptides on a graphite surface, Langmuir the ACS journal of surfaces and colloids 39 (2023) 7057–7062.

[32] Y. Qian, S. Di, L. Wang, Z. Li, Recent advances in the synthesis and applications of graphene-polypeptide nanocomposites, J. Mater. Chem. B 9 (2021) 6521–6535.

[33] R. Teixeira-Santos, S. Belo, R. Vieira, F.J.M. Mergulhão, L.C. Gomes, Graphene-Based composites for biomedical applications: surface modification for enhanced antimicrobial activity and biocompatibility, Biomolecules 13 (2023).

[34] B.A.E. Lehner, D. Benz, S.A. Moshkalev, A.S. Meyer, M.A. Cotta, R. Janissen, Biocompatible graphene oxide nanosheets densely functionalized with biologically active molecules for biosensing applications, ACS Appl. Nano Mater. 4 (2021) 8334–8342.

[35] N. Alvisi, R. de Vries, Biomedical applications of solid-binding peptides and proteins, Mater. Today Bio 19 (2023) 100580.

[36] Y. Cui, S.N. Kim, S.E. Jones, L.L. Wissler, R.R. Naik, M.C. McAlpine, Chemical functionalization of graphene enabled by phage displayed peptides, Nano Lett. 10 (2010) 4559–4565.

[37] C.R. So, Y. Hayamizu, H. Yazici, C. Gresswell, D. Khatayevich, C. Tamerler, M. Sarikaya, Controlling self-assembly of engineered peptides on graphite by rational mutation, ACS Nano 6 (2012) 1648–1656.

[38] X. Mao, Y. Wang, L. Liu, L. Niu, Y. Yang, C. Wang, Molecular-level evidence of the surface-induced transformation of peptide structures revealed by scanning tunneling microscopy, Langmuir the ACS journal of surfaces and colloids 25 (2009) 8849–8853.

[39] X. Mao, Y. Guo, Y. Luo, L. Niu, L. Liu, X. Ma, H. Wang, Y. Yang, G. Wei, C. Wang, Sequence effects on peptide assembly characteristics observed by using scanning tunneling microscopy, J. Am. Chem. Soc. 135 (2013) 2181–2187.

[40] B. Sapkota, A. Benabbas, H.-Y.G. Lin, W. Liang, P. Champion, M. Wanunu, Peptide-Decorated tunable-fluorescence Graphene Quantum dots, ACS applied materials & interfaces 9 (2017) 9378–9387.

[41] X. Dang, H. Yi, M.-H. Ham, J. Qi, D.S. Yun, R. Ladewski, M.S. Strano, P. T. Hammond, A.M. Belcher, Virus-templated self-assembled single-walled carbon nanotubes for highly efficient electron collection in photovoltaic devices, Nat. Nanotechnol. 6 (2011) 377–384.

[42] P. Li, K. Sakuma, S. Tsuchiya, L. Sun, Y. Hayamizu, Fibroin-like peptides self-assembling on two-dimensional materials as a molecular scaffold for potential biosensing, ACS Appl. Mater. Interfaces 11 (2019) 20670–20677.

[43] M.J. Pender, L.A. Sowards, J.D. Hartgerink, M.O. Stone, R.R. Naik, Peptide-mediated formation of single-wall carbon nanotube composites, Nano Lett. 6 (2006) 40–44.

[44] D. Nii, Y. Nozawa, M. Miyachi, Y. Yamanoi, H. Nishihara, T. Tomo, Y. Shimada, Peptide aptamer-assisted immobilization of green fluorescent protein for creating biomolecule-complexed carbon nanotube device, Jpn. J. Appl. Phys. 56 (2017) 107001.

[45] M. Wang, T. Yang, Q. Bao, M. Yang, C. Mao, Binding peptide-promoted biofunctionalization of graphene paper with hydroxyapatite for stimulating osteogenic differentiation of mesenchymal stem cells, ACS applied materials & interfaces 14 (2022) 350–360.

[46] M. Mao, L. Ahrens, J. Luka, F. Contreras, T. Kurkina, M. Bienstein, M. Sária Pereira de Passos, G. Schirinzi, D. Mehn, A. Valsesia, C. Desmet, M.-Á. Serra, D. Gilliland, U. Schwaneberg, Material-specific binding peptides empower sustainable innovations in plant health, biocatalysis, medicine and microplastic quantification, Chem. Soc. Rev. 53 (2024) 6445–6510.

[47] A. Care, P.L. Bergquist, A. Sunna, Solid-binding peptides: smart tools for nanobiotechnology, Trends Biotechnol. 33 (2015) 259–268.

[48] U. Kriplani, B.K. Kay, Selecting peptides for use in nanoscale materials using phage-displayed combinatorial peptide libraries, Curr. Opin. Biotechnol. 16 (2005) 470–475.

[49] U.O.S. Seker, H.V. Demir, Material binding peptides for nanotechnology, Molecules 16 (2011) 1426–1451.

[50] L. Apitius, S. Buschmann, C. Bergs, D. Schönauer, F. Jakob, A. Pich, U. Schwaneberg, Biadhesive peptides for assembling stainless steel and compound loaded micro-containers, Macromol. Biosci. 19 (2019) e1900125.

[51] J. Dittrich, C. Brethauer, L. Goncharenko, J. Bührmann, V. Zeisler-Diehl, S. Pariyar, F. Jakob, T. Kurkina, L. Schreiber, U. Schwaneberg, H. Gohlke, Rational design yields molecular insights on leaf-binding of anchor peptides, ACS Appl. Mater. Interfaces 14 (2022) 28412–28426.

[52] A.M.C. Maan, C.N. Graafsma, A.H. Hofman, T. Pelras, W.M. de Vos, M. Kamperman, Scalable fabrication of reversible antifouling block copolymer coatings via adsorption strategies, ACS Appl. Mater. Interfaces 15 (2023) 19682–19694.

[53] F. Yang, H.E. Kadaoui, J. Gebauer, D.D.A. Basaran, L. Stauder, S. Barth, T. Bergs, U. Schwaneberg, Investigation of the potential of dipping as a technology for bifunctional assemblies as a coating material, Proced. CIRP 121 (2024) 186–191.

[54] H. Cui, L. Zhang, D. Söder, X. Tang, M.D. Davari, U. Schwaneberg, Rapid and oriented immobilization of laccases on electrodes via a methionine-rich peptide, ACS Catal. 11 (2021) 2445–2453.

[55] C. Nenninger, F. Contreras, M. Vorobii, M. Sária Pereira de Passos, J. Gebauer, M. Nöth, L. Stütgens, H. El Kadaoui, T. Bergs, U. Schwaneberg, Surface-confined enzymatic method for scalable thin film generation, Surf. Interfaces 60 (2025) 106046.

[56] T. Xu, E. Telser, R.F. Troxler, F.G. Oppenheim, Primary structure and anticandidal activity of the major histatin from parotid secretion of the subhuman primate, Macaca fascicularis, Journal of dental research 69 (1990) 1717–1723.
[57] M. Varadi, D. Bertoni, P. Magana, U. Paramval, I. Pidruchna, M. Radhakrishnan, M. Tsenkov, S. Nair, M. Mirdita, J. Yeo, O. Kovalevskiy, K. Tunyasuvunakool, A. Laydon, A. Žídek, H. Tomlinson, D. Hariharan, J. Abrahamson, T. Green, J. Jumper, E. Birney, M. Steinegger, D. Hassabis, S. Velankar, AlphaFold Protein Structure Database in 2024: providing structure coverage for over 214 million protein sequences, Nucleic acids research 52 (2024) D368–D375.
[58] Y. Lu, K.-W. Hintzen, T. Kurkina, Y. Ji, U. Schwaneberg, Directed evolution of material binding peptide for polylactic acid-specific degradation in mixed plastic wastes, ACS Catal. 13 (2023) 12746–12754.
[59] P.W. Iversen, B. Beck, Y.-F. Chen, W. Dere, V. Devanarayan, B.J. Eastwood, M. W. Farmen, S.J. Iturria, C. Montrose, R.A. Moore, J.R. Weidner, G.S. Sittampalam, HTS assay validation, in: S. Markossian, A. Grossman, M. Arkin, et al. (Eds.), Assay Guidance Manual [Internet], Eli Lilly & Company and the National Center for Advancing Translational Sciences, Bethesda (MD), 2004.
[60] K. Bitar, J.G. Reinhold, Phytase and alkaline phosphatase activities in intestinal mucosae of rat, chicken, calf, and man, Biochim. Biophys. Acta 268 (1972) 442–452.
[61] J.B. Garrett, K.A. Kretz, E. O'Donoghue, J. Kerovuo, W. Kim, N.R. Barton, G. P. Hazlewood, J.M. Short, D.E. Robertson, K.A. Gray, Enhancing the thermal tolerance and gastric performance of a microbial phytase for use as a phosphate-mobilizing monogastric-feed supplement, Appl. Environ. Microbiol. 70 (2004) 3041–3046.
[62] A.P. Jacobus, J. Gross, Optimal cloning of PCR fragments by homologous recombination in Escherichia coli, PLoS One 10 (2015) e0119221.
[63] K. Miyazaki, MEGAWHOP cloning: a method of creating random mutagenesis libraries via megaprimer PCR of whole plasmids, Methods Enzymol. 498 (2011) 399–406.
[64] F.W. Studier, Protein production by auto-induction in high density shaking cultures, Protein Expr. Purif. 41 (2005) 207–234.
[65] A. Reina, X. Jia, J. Ho, D. Nezich, H. Son, V. Bulovic, M.S. Dresselhaus, J. Kong, Large area, few-layer graphene films on arbitrary substrates by chemical vapor deposition, Nano Lett. 9 (2009) 30–35.
[66] M.-A. Yoon, C. Kim, J.-H. Kim, H.-J. Lee, K.-S. Kim, Surface properties of CVD-Grown graphene transferred by wet and dry transfer processes, Sensors (Basel, Switzerland) 22 (2022).
[67] U. Schwaneberg, Created in Biorender, 2026.
[68] H. Steiner, D. Hultmark, A. Engström, H. Bennich, H.G. Boman, Sequence and specificity of two antibacterial proteins involved in insect immunity, Nature 292 (1981) 246–248.
[69] X. Gong, G. Liu, Y. Li, D.Y.W. Yu, W.Y. Teoh, Functionalized-Graphene composites: fabrication and applications in sustainable energy and environment, Chem. Mater. 28 (2016) 8082–8118.
[70] T. Osaki, M. Omotezako, R. Nagayama, M. Hirata, S. Iwanaga, J. Kasahara, J. Hattori, I. Ito, H. Sugiyama, S. Kawabata, Horseshoe crab hemocyte-derived antimicrobial polypeptides, tachystatins, with sequence similarity to spider neurotoxins, J. Biol. Chem. 274 (1999) 26172–26178.
[71] S.N. Kim, Z. Kuang, J.M. Slocik, S.E. Jones, Y. Cui, B.L. Farmer, M.C. McAlpine, R. R. Naik, Preferential binding of peptides to graphene edges and planes, J. Am. Chem. Soc. 133 (2011) 14480–14483.
[72] S.S. Kim, Z. Kuang, Y.H. Ngo, B.L. Farmer, R.R. Naik, Biotic-Abiotic interactions: factors that influence peptide-graphene interactions, ACS Appl. Mater. Interfaces 7 (2015) 20447–20453.
[73] A.E. Islam, R. Martineau, C.M. Crasto, H. Kim, R.S. Rao, B. Maruyama, S.S. Kim, L. F. Drummy, Graphene-Based electrolyte-gated field-effect transistors for potentiometrically sensing neuropeptide Y in physiologically relevant environments, ACS Appl. Nano Mater. 3 (2020) 5088–5097.
[74] S.M. Thomas, H. Zhang, K. Wang, M.R. Knecht, T.R. Walsh, Exploiting materials binding peptides for the Organization of Resilient Biomolecular constructs, Biomacromolecules 25 (2024) 7216–7224.
[75] A.V. Shivange, A. Dennig, U. Schwaneberg, Multi-site saturation by OmniChange yields a pH- and thermally improved phytase, J. Biotechnol. 170 (2014) 68–72.
[76] A.M. Waterhouse, J.B. Procter, D.M.A. Martin, M. Clamp, G.J. Barton, Jalview Version 2–a multiple sequence alignment editor and analysis workbench, Bioinformatics (Oxford, England) 25 (2009) 1189–1191.
[77] R.B. Pandey, Z. Kuang, B.L. Farmer, S.S. Kim, R.R. Naik, Stability of peptide (P1 and P2) binding to a graphene sheet via an all-atom to all-residue coarse-grained approach, Soft Matter 8 (2012) 9101.
[78] D. Shukla, B.L. Trout, Interaction of arginine with proteins and the mechanism by which it inhibits aggregation, The journal of physical chemistry. B 114 (2010) 13426–13438.
[79] E. Wu, M.-O. Coppens, S. Garde, Role of arginine in mediating protein-carbon nanotube interactions, Langmuir the ACS journal of surfaces and colloids 31 (2015) 1683–1692.
[80] L. Zhang, Y. Sheng, A. Zehtab Yazdi, K. Sarikhani, F. Wang, Y. Jiang, J. Liu, T. Zheng, W. Wang, P. Ouyang, P. Chen, Surface-assisted assembly of a histidine-rich lipidated peptide for simultaneous exfoliation of graphite and functionalization of graphene nanosheets, Nanoscale 11 (2019) 2999–3012.
[81] K. Rübsam, M.D. Davari, F. Jakob, U. Schwaneberg, KnowVolution of the polymer-binding peptide LCI for improved polypropylene binding, Polymers 10 (2018).
[82] D. Horinek, A. Serr, M. Geisler, T. Pirzer, U. Slotta, S.Q. Lud, J.A. Garrido, T. Scheibel, T. Hugel, R.R. Netz, Peptide adsorption on a hydrophobic surface results from an interplay of solvation, surface, and intrapeptide forces, Proc. Natl. Acad. Sci. U. S. A 105 (2008) 2842–2847.
[83] Y. Kumada, D. Kuroki, H. Yasui, T. Ohse, M. Kishimoto, Characterization of polystyrene-binding peptides (PS-tags) for site-specific immobilization of proteins, J. Biosci. Bioeng. 109 (2010) 583–587.
[84] Y. Hong, S. Najafi, T. Casey, J.-E. Shea, S.-I. Han, D.S. Hwang, Hydrophobicity of arginine leads to reentrant liquid-liquid phase separation behaviors of arginine-rich proteins, Nat. Commun. 13 (2022) 7326.
[85] D. Söder, M. Garay-Sarmiento, K. Rahimi, F. Obstals, S. Dedisch, T. Haraszti, M. D. Davari, F. Jakob, C. Heß, U. Schwaneberg, C. Rodriguez-Emmenegger, Unraveling the mechanism and kinetics of binding of an LCI-eGFP-Polymer for antifouling coatings, Macromol. Biosci. 21 (2021) e2100158.
[86] S. Bräse, J. Bülle, A. Hüttermann, Organische Und Bioorganische Chemie: Das Basiswissen Für Master- Und Diplomprüfungen, Wiley-VCH, Weinheim, 2008.
[87] D. Fu, H. Huang, H. Luo, Y. Wang, P. Yang, K. Meng, Y. Bai, N. Wu, B. Yao, A highly pH-stable phytase from Yersinia kristeensenii: cloning, expression, and characterization, Enzym. Microb. Technol. 42 (2008) 499–505.
[88] S. Wang, J. Gao, X. Chu, Residue-Specific structural and dynamical coupling of protein and hydration water revealed by molecular dynamics simulations, Biomolecules 15 (2025) 660.
[89] K.K. Lee, C.A. Fitch, J.T.J. Lecomte, B. García-Moreno E, Electrostatic effects in highly charged proteins: salt sensitivity of pKa values of histidines in staphylococcal nuclease, Biochemistry 41 (2002) 5656–5667.
[90] M. Thi Hong Nguyen, M. Vazdar, Molecular dynamics simulations unveil the aggregation patterns and salting out of polyarginines at zwitterionic POPC bilayers in solutions of various ionic strengths, Comput. Struct. Biotechnol. J. 23 (2024) 3897–3905.
[91] A. Akaishi, T. Yonemaru, J. Nakamura, Formation of water layers on graphene surfaces, ACS Omega 2 (2017) 2184–2190.
[92] H. Jalali, E. Lotfi, R. Boya, M. Neek-Amal, Abnormal dielectric constant of nanoconfined water between graphene layers in the presence of salt, The journal of physical chemistry. B 125 (2021) 1604–1610.
[93] S. Yang, X. Zhao, Y.-H. Lu, E.S. Barnard, P. Yang, A. Baskin, J.W. Lawson, D. Prendergast, M. Salmeron, Nature of the electrical double layer on suspended graphene electrodes, J. Am. Chem. Soc. 144 (2022) 13327–13333.
[94] J.D. Bloom, F.H. Arnold, In the light of directed evolution: pathways of adaptive protein evolution, Proc. Natl. Acad. Sci. U. S. A 106 (Suppl 1) (2009) 9995–10000.
[95] D. Khatayevich, T. Page, C. Gresswell, Y. Hayamizu, W. Grady, M. Sarikaya, Selective detection of target proteins by peptide-enabled graphene biosensor, Small 10 (2014), 1505-13, 1504.
[96] L. Wang, Y. Zhang, A. Wu, G. Wei, Designed graphene-peptide nanocomposites for biosensor applications: a review, Anal. Chim. Acta 985 (2017) 24–40.